Second-Harmonic Coherent Driving of a Spin Qubit in a Si/SiGe Quantum Dot

P. Scarlino,[1] E. Kawakami,[1] D. R. Ward,[2] D. E. Savage,[2] M. G. Lagally,[2] Mark Friesen,[2] S. N. Coppersmith,[2] M. A. Eriksson,[2] and L. M. K. Vandersypen[1,*]

[1]*Kavli Institute of Nanoscience, TU Delft, Lorentzweg 1, 2628 CJ Delft, Netherlands*

[2]*University of Wisconsin-Madison, Madison, Wisconsin 53706, USA*

(Received 24 April 2015; published 1 September 2015)

We demonstrate coherent driving of a single electron spin using second-harmonic excitation in a Si/SiGe quantum dot. Our estimates suggest that the anharmonic dot confining potential combined with a gradient in the transverse magnetic field dominates the second-harmonic response. As expected, the Rabi frequency depends quadratically on the driving amplitude, and the periodicity with respect to the phase of the drive is twice that of the fundamental harmonic. The maximum Rabi frequency observed for the second harmonic is just a factor of 2 lower than that achieved for the first harmonic when driving at the same power. Combined with the lower demands on microwave circuitry when operating at half the qubit frequency, these observations indicate that second-harmonic driving can be a useful technique for future quantum computation architectures.

DOI: 10.1103/PhysRevLett.115.106802 PACS numbers: 73.21.La, 71.70.Ej, 72.25.Rb, 75.70.Tj

Controlled two-level quantum systems are essential elements for quantum information processing. A natural and archetypical controlled two-level system is the electron spin doublet in the presence of an external static magnetic field [1,2]. The common method for driving transitions between the two spin states is magnetic resonance, whereby an ac magnetic field (B_{ac}) is applied transverse to the static magnetic field (B_{ext}), with a frequency, f_{MW}, matching the spin Larmor precession frequency $f_L = g\mu_B B_{\mathrm{tot}}/h$ (h is Planck's constant, μ_B is the Bohr magneton, and B_{tot} the total magnetic field acting on the spin). Coherent rotations of the spin, known as Rabi oscillations, can be observed when driving overcomes decoherence.

Both spin transitions and Rabi oscillations can be driven not just at the fundamental harmonic, but also at higher harmonics, i.e., where the frequency of the transverse ac field is an integer fraction of the Larmor frequency, $f_{\mathrm{MW}} = f_L/n$, with n an integer. Second or higher harmonic generation involves nonlinear phenomena. Such processes are well known and explored in quantum optics using nonlinear crystals [3], and their selectivity for specific transitions is exploited in spectroscopy and microscopy [4–8]. Two-photon coherent transitions have also been extensively explored for biexcitons in (In,Ga)As quantum dots [9] and in superconducting qubit systems [10–13]. In cavity QED systems, a two-photon process has the advantage that it allows the direct transition from the ground state to the second excited state, which is forbidden in the dipole transition by the selection rules [14].

For electron spin qubits, it has been predicted that the nonlinear dependence of the g tensor on applied electric fields should allow electric-dipole spin resonance at subharmonics of the Larmor frequency for hydrogenic donors in a semiconductor [15,16]. For electrically driven spin qubits confined in a (double) quantum dot, higher-harmonic driving has been proposed that takes advantage of an anharmonic dot confining potential [17–21] or a spatially inhomogeneous magnetic field [22]. In order to use higher harmonic generation for coherent control of a system, the corresponding driving rate must exceed the decoherence rate. This requires a nonlinearity that is sufficiently strong. Although weak nonlinearities are easily obtained and have allowed higher harmonics to be used in continuous wave (cw) spectroscopy for quantum dots hosted in GaAs, InAs, InSb, and carbon nanotubes [23–28], coherent spin manipulation using higher harmonics has not been demonstrated previously.

In this Letter, we present experimental evidence of coherent second-harmonic manipulation of an electron spin confined in a single quantum dot (QD) hosted in a Si/SiGe quantum well. We show that this second-harmonic driving can be used for universal spin control, and we use it to measure the free-induction and Hahn-echo decay of the electron spin. Furthermore, we study how the second-harmonic response varies with the microwave amplitude and phase, and comment on the nature of the nonlinearity that mediates the second-harmonic driving process in this system.

The quantum dot is electrostatically induced in an undoped Si/SiGe quantum well structure, through a combination of accumulation and depletion gates (see Sec. I of [29] for full details). The sample and the settings are the same as those used in Ref. [30]. A cobalt micromagnet next to the QD creates a local magnetic field gradient, enabling spin transitions to be driven by electric fields [30,31].

All measurements shown here are performed using single-shot readout via a QD charge sensor [32]. They make use of four-stage gate voltage pulses implementing (1) initialization to spin-down, (2) spin manipulation through all-electrical

microwave excitation, (3) single-shot spin readout, and (4) a compensation or empty stage [30]. The results of many single-shot cycles are used to determine the spin-up probability, $P_\uparrow$, at the end of the manipulation stage.

First, we apply long, low-power microwave excitation to perform quasi-cw spectroscopy. Figure 1(a) shows four observed spin resonance frequencies, $f_0^{(1)}$ through $f_0^{(4)}$, as a function of the external magnetic field. The resonances labeled (1) and (2) represent the response at the fundamental frequency. As in [30], these two closely spaced resonances correspond to the electron occupying either of the two lowest valley states, both of which are thermally

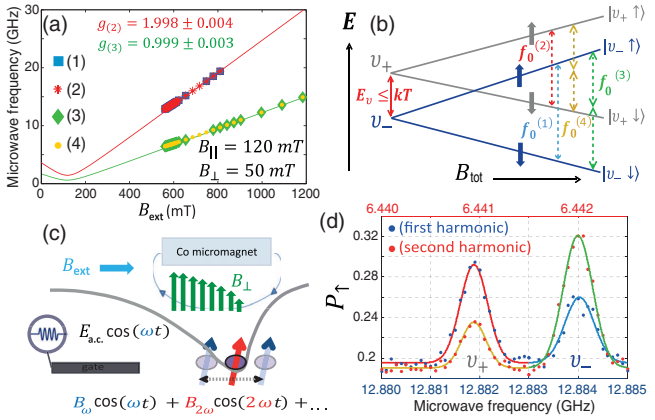

FIG. 1 (color). (a) Measured resonance frequencies as a function of externally applied magnetic field $B_{\rm ext}$. The long microwave burst time $t_p = 700\ \mu s \gg T_2^*$ means that the applied excitation is effectively continuous wave. The microwave source output power was $P = -33$ dBm to -10 dBm (-20 dBm to -5 dBm) for the case of fundamental (second) harmonic excitation, decreasing for lower microwave frequency in order to avoid power broadening. The red and green lines represent fits with the relation $hf = g\mu_B\sqrt{(B_{\rm ext} - B_\parallel)^2 + B_\perp^2}$, respectively, to the resonance data labeled (2) and (3) (we excluded points with $B_{\rm ext} < 700$ mT from the fit because the micromagnet apparently begins to demagnetize there) [30]. (b) Schematic of the energy levels involved in the excitation process, as a function of the total magnetic field at the electron location. The dashed arrows correspond to the four transitions in panel (a), using the same color code. (c) Schematic of an anharmonic confinement potential, leading to higher harmonics in the electron oscillatory motion in response to a sinusoidally varying excitation. (d) Measured spin-up probability, $P_\uparrow$, as a function of applied microwave frequency, $f_{\rm MW}$, for $B_{\rm ext} = 560.783$ mT ($P = -30$ dBm for the fundamental response, $P = -12$ dBm for the second harmonics), averaged over 150 repetitions per point times 80 repeated frequency sweeps (160 mins in total). The frequency axis (in red on top) has been stretched by a factor of 2 for the second-harmonic spin response (red data points). From the linewidths, we extract a lower bound for the dephasing time $T_2^{*(1)} = 760 \pm 100$ ns, $T_2^{*(2)} = 810 \pm 50$ ns, $T_2^{*(3)} = 750 \pm 40$ ns and $T_2^{*(4)} = 910 \pm 80$ ns. The Gaussian fits through the four peaks use the same color code as in panels (a) and (b).

populated here. The other two resonances occur at exactly half the frequency of the first two, $f_0^{(1)} = 2f_0^{(3)}$, $f_0^{(2)} = 2f_0^{(4)}$, and represent the second-harmonic response.

The effective g factors extracted from the slopes for the second-harmonic response are half those for the first-harmonic response [see Fig. 1(a), inset]. The relevant energy levels and transitions as a function of the total magnetic field, $B_{\rm tot}$, are visualized in Fig. 1(b), where the color scheme used for the resonances is the same as in Fig. 1(a). We see two sets of Zeeman split doublets, separated by the splitting between the two lowest-energy valleys, E_v. The transition between the Zeeman sublevels within each doublet can be driven by absorbing a single photon (1 ph) or two photons (2 ph), as indicated by the single and double arrows.

To drive a transition using the second harmonic, a nonlinearity is required. In principle, several mechanisms can introduce such a nonlinearity in this system (see Sec. II of [29]). First, as schematically shown in Fig. 1(c), if the confining potential is anharmonic, an oscillating electric field of amplitude $E_{\rm ac}$ and angular frequency $\omega = 2\pi f_{\rm MW}$ induces effective displacements of the electron wave function with spectral components at angular frequencies $n\omega$, with n an integer. In analogy with nonlinear optical elements, we can look at this process as generated by an effective nonlinear susceptibility of the electron bounded to the anharmonic QD confinement potential.

The gradient in the transverse magnetic field in the dot region ($B_\perp$ in green) converts the electron motion into an oscillating transverse magnetic field of the form

$$B_\perp^{\rm ac}(t) = B_\omega \cos(\omega t) + B_{2\omega}\cos(2\omega t) + \cdots, \qquad (1)$$

that can drive the electron spin for $\hbar\omega = E_z$, $2\hbar\omega = E_z$, and so forth [17]. A possible source of anharmonicity arises from the nonlinear dependence of the dipole moment between the valley (or valley-orbit) ground (υ_-) and excited states (υ_+) [33], as a function of $E_{\rm ac}$.

A second possible source of nonlinearity is a variation of the transverse field gradient, $(dB_\perp/dx, dy)$, with position [see Fig. 1(c)]. Even if the confining potential were harmonic, this would still lead to an effective transverse magnetic field containing higher harmonics, of the same form as Eq. (1).

A third possibility is that not only the transverse magnetic field, but also the longitudinal magnetic field varies with position. This leads to an ac magnetic field which is not strictly perpendicular to the static field, which is, in itself, sufficient to allow second-harmonic driving [21,34,35], even when the confining potential is harmonic and the field gradients are constant over the entire range of the electron motion.

However, simple estimates indicate that the second and third mechanisms are not sufficiently strong in the present sample to allow the coherent spin manipulation we report below (see Sec. II of [29]). We propose that the first

mechanism is dominant in this sample, supported by our observation that the strength of the second-harmonic response is sensitive to the gate voltages defining the dot.

In Fig. 1(d), we zoom in on the four cw spin resonance peaks, recorded at low enough power to avoid power broadening (see Sec. I of [29]). Fitting those resonances with Gaussian relation, we extract the dephasing times $T_2^{*,(1,2)} = [\sqrt{2}\hbar/\pi\delta f_{\mathrm{FWHM}}^{(1,2)}]$, $T_2^{*,(3,4)} = [\sqrt{2}\hbar/2\pi\delta f_{\mathrm{FWHM}}^{(3,4)}]$, giving values in the range of 750 to 910 ns for all four resonances [see caption of Fig. 1(d)]. This directly shows that the linewidth (FWHM) extracted for the two-photon process is half that for the one-photon process, as expected [15,22,35].

From the relative peak heights in Fig. 1(d), we can estimate the ratio of the Rabi frequencies between the two peaks in each pair (see Sec. I of [29]). In [30], we found that the relative thermal populations of the two valleys ($\epsilon^{(4)}/\epsilon^{(3)}$) were about 0.3 ± 0.1 to 0.7 ± 0.1. Given this, the ratio between the Rabi frequencies, f_1, extracted from the peak heights is $r_R(2\ \mathrm{ph}) = f_1^{(4)}/f_1^{(3)} = 0.9 \pm 0.2$ for the second harmonics. This is different from the ratio observed in [30] for the fundamental harmonic, $r_R(1\ \mathrm{ph}) = f_1^{(2)}/f_1^{(1)} = 1.70 \pm 0.05$ [36].

Such a difference is to be expected. The ratio $r_R(2\ \mathrm{ph})$ is affected by how the degree of anharmonicity in the confining potential differs between the two valleys. In contrast, $r_R(1\ \mathrm{ph})$ depends on how the electrical susceptibility differs between the two valleys [37]. In addition, since the valleys have different charge distributions [33], the microwave electric field couples differently to the two valley states, and this difference can be frequency dependent [38,39]. Because the second-harmonic Rabi oscillations are driven at half the frequency of the Rabi oscillations driven at the fundamental, this frequency dependence also contributes to a difference between $r_R(1\ \mathrm{ph})$ and $r_R(2\ \mathrm{ph})$. We note that the difference in Rabi frequency ratio between the 1-photon and 2-photon case demonstrates that the second-harmonic response is not just the result of a classical up-conversion of the microwave frequency taking place before the microwave radiation impinges on the dot, but takes place at the dot itself.

The second-harmonic response also permits coherent driving, for which a characteristic power dependence is expected [22,35,40]. Figure 2(a) shows Rabi oscillations, where the microwave burst time is varied keeping $f_{\mathrm{MW}} = f_0^{(3)}$ for different microwave powers. We note that the contribution to the measured spin-up oscillations coming from the other resonance, (4), is negligible because the respective spin Larmor frequencies are off resonance by 2 MHz, $f_1^{(3)}/f_1^{(4)} \approx 1$ and its population is $\sim$ three times smaller.

To analyze the dependence of the Rabi frequency on microwave power, we perform a FFT of various sets of Rabi oscillations similar to those in Fig. 2(a). Figure 2(b) shows the Rabi frequency thus obtained versus microwave power

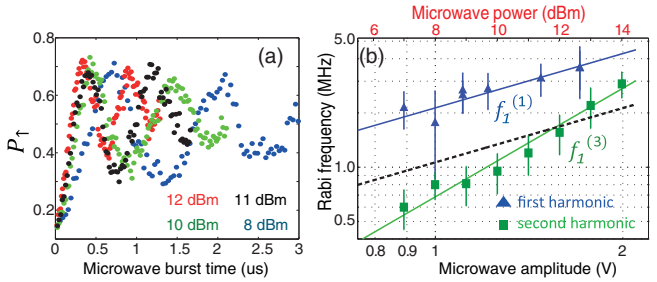

FIG. 2 (color). Rabi oscillations. (a) Measured spin-up probability, $P_\uparrow$, as a function of microwave burst time ($B_{\mathrm{ext}} = 560.783$ mT, $f_{\mathrm{MW}} = 6.4455$ GHz) at four different microwave powers, corresponding to a rms voltage at the source of 998.8 mV, 1257.4 mV, 1410.9 mV, 1583.0 mV. (b) Rabi frequencies recorded at the fundamental harmonic, $f_0^{(1)}$ (blue triangles, adapted from [30]), and at the second harmonic, $f_0^{(3)}$ (green squares), as a function of the microwave amplitude emitted from the source (top axis shows the corresponding power). For the second harmonic, the amplitude shown corresponds to a 5 dB higher power than the actual output power, to compensate for the 5 dB lower attenuation of the transmission line at 6 GHz versus 12 GHz (estimated by measuring the coax transmission at room temperature). The green solid (dashed black) line is a fit of the second-harmonic data with the relation $\log(f^R) \propto 2\log(E_{\mathrm{ac}})$ [$\log(f^R) \propto \log(E_{\mathrm{ac}})$]. The large error bars in the FFT of the data in Fig. 2(a) arise because we perform the FFT on only a few oscillations. $B_{\mathrm{ext}} = 560.783$ mT.

for driving both at the second harmonic (green) and at the fundamental (blue), taken for identical dot settings [30]. We see that for driving at the frequency of the second harmonic, the Rabi frequency is quadratic in the applied electric field amplitude (linear in power), as expected from theory [22,35,40]. When driving at the fundamental resonance, the Rabi frequency is linear in the driving amplitude, as usual. It is worth noting that, at the highest power used in this experiment, the Rabi frequency obtained from driving the fundamental valley-orbit ground state spin resonance is just a factor of 2 higher than the one from driving at the second harmonic. This ratio indicates that the use of second-harmonic driving is quite efficient in our device. This result is consistent with Ref. [22], which shows that Rabi frequencies at subharmonic resonances can be comparable to the Rabi frequency at the fundamental resonance and, also, with the theory and experiments in Refs. [20] and [26], which report resonant response at a second harmonic that can exceed that at the fundamental.

A further peculiarity in coherent driving using second harmonics is seen when we vary the phase of two consecutive microwave bursts. Figure 3(a) shows the spin-up probability following two $\pi/2$ microwave bursts with relative phase $\Delta\phi$, resonant with $f_0^{(3)}$ and separated by a fixed waiting time τ. For short τ, the signal oscillates sinusoidally in $\Delta\phi$ with a period that is half that for the single-photon case [compare the black traces in Figs. 3(a) and 3(b)].

Therefore, in order to rotate the electron spin around an axis in the rotating frame rotated by 90° with respect to a

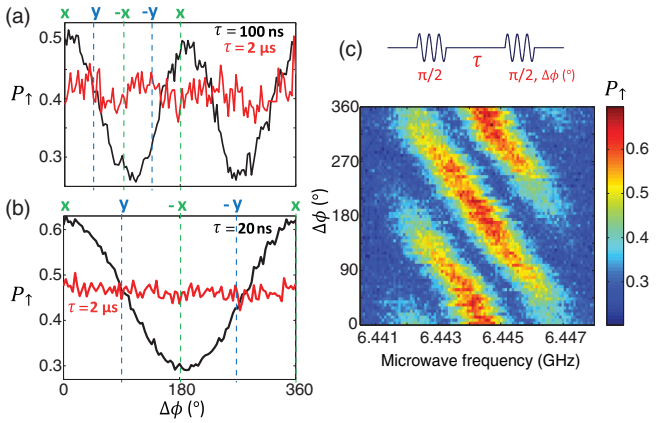

FIG. 3 (color). Phase control of oscillations. (a) Probability $P_\uparrow$ measured after applying two $\pi/2$ rotations via second-harmonic excitation, as a function of the relative phase between the two microwave bursts, $\Delta\phi$. The two rotations are separated by $\tau =$ 100 ns (black) and $\tau = 2\ \mu$s (red). ($P = 16.0$ dBm, $B_{\text{ext}} =$ 560.783 mT, $f_{\text{MW}} = f_0^{(3)} = 6.44289$ GHz). (b) Similar to panel (a), but now driving the fundamental harmonic for $\tau = 20$ ns (black) and $\tau = 2\,\mu$s (red). ($P = 12.0$ dBm, $B_{\text{ext}} = 560.783$ mT, $f_{\text{MW}} = f_0^{(2)} = 12.88577$ GHz). Inset: Microwave pulse scheme used for this measurement. (c) Measured spin-up probability, $P_\uparrow$ (1000 repetitions for each point), as a function of f_{MW} and the relative phase $\Delta\phi$ between two $\pi/2$ microwave bursts (130 ns, $P = 16.0$ dBm) for second-harmonic excitation, with $\tau = 50$ ns. The measurement extends over more than 15 hours.

prior spin rotation axis (e.g., a Y rotation following an X rotation in the rotating frame), we need to set $\Delta\phi$ to 45°, instead of 90°, when driving via the second harmonic. Of course, for $\tau \gg T_2^*$, the contrast has vanished, indicating that all phase information is lost during the waiting time [Figs. 3(a) and 3(b) red traces]. Figure 3(c) shows two-pulse measurements, as in Fig. 3(a), as a function of frequency detuning and phase difference, where we can appreciate the extraordinary stability of the undoped device.

To probe further the coherence properties of the spin, we perform a free induction (Ramsey) decay measurement, see Fig. 4(a), as a function of frequency detuning and delay time, τ, between the two bursts. The absence of a central frequency symmetry axis is due to the presence of two superimposed oscillating patterns, originating from the resonances at $f_0^{(3)}$ and $f_0^{(4)}$. Figures 4(c)–4(e) show sections of the Ramsey measurement in Fig. 4(a), corresponding to different waiting times τ (see the white dashed lines). The visibility of the Ramsey fringes clearly decreases for longer waiting times between the two $\pi/2$ pulses. Fitting the decay of the visibility of the fringes as a function of τ with a Gaussian [$\propto \exp[-(t/T_2^*)^2]$, see Sec. I of [29]], we find $T_2^* = 780 \pm 110$ ns, in agreement with the value extracted from the linewidth.

Furthermore, and analogously to the observations of Fig. 3(a), we report a doubling effect in the frequency of the Ramsey oscillations, f_{Ramsey}, as a function of the detuning

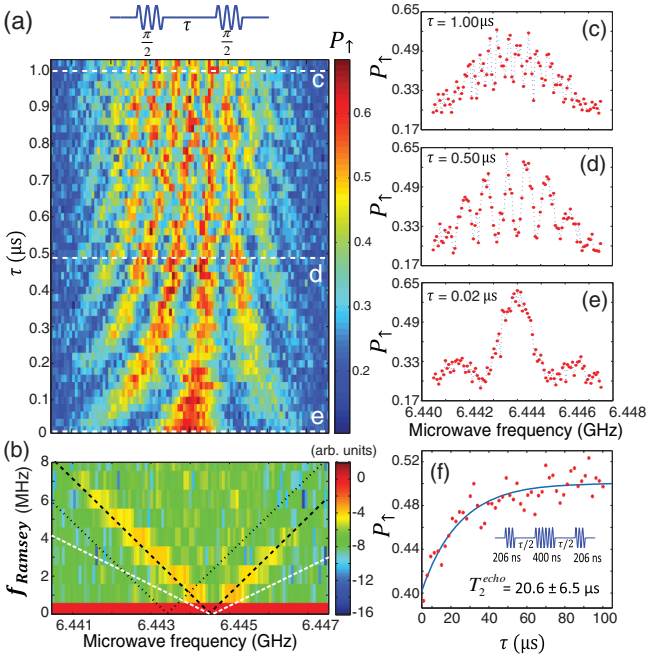

FIG. 4 (color). Ramsey fringes. (a) Measured spin-up probability, $P_\uparrow$, as a function of f_{MW} and waiting time τ ($B_{\text{ext}} = 560.783$ mT, $P = 13.0$ dBm) between two $\pi/2$ pulses (130 ns) with equal phase, showing Ramsey interference. Each data point is averaged over 300 cycles. Inset: Microwave pulse scheme used for this measurement. (b) Fourier transform over the waiting time, τ, of the data in panel (a), showing a linear dependence on the microwave frequency, with vertex at $f_{\text{MW}} = f_0^{(3)}$ and slope $f_{\text{Ramsey}} = 2\Delta f_{\text{MW}}$ (black dashed lines). The expected position of the FFT of the signal arising from resonance $f_0^{(4)}$ is indicated by the dotted black line. For comparison, the white dashed line represents the relation $f_{\text{Ramsey}} = \Delta f_{\text{MW}}$. (c)–(e) Sections of the Ramsey interference pattern in (a) along the three white dashed lines; the respective waiting times are indicated also in the inset of each panel. (f) Measured spin-up probability as a function of the total free evolution time, τ, in a Hahn echo experiment (pulse scheme shown in inset). The decay curve is fit well to a single exponential (blue). Here, $f_{\text{MW}} = f_0^{(3)}$, $B_{\text{ext}} = 560.783$ mT.

$\Delta f_{\text{MW}} = f_{\text{MW}} - f_0^{(3)}$. Figure 4(b) shows $f_{\text{Ramsey}}(\Delta f_{\text{MW}})$, extracted from the data in Fig. 4(a) via a FFT over the waiting time τ. The black dashed line indicates the condition $f_{\text{Ramsey}} = 2\Delta f_{\text{MW}}$, closely overlapping with the position of the yellow peaks in the FFT. The black dotted line indicates the condition $f_{\text{Ramsey}} = 2(f_{\text{MW}} - f_0^{(4)})$; this second resonance is not very visible in the data, due to the lower population of the corresponding valley. For comparison, the white dashed line indicates the condition $f_{\text{Ramsey}} = \Delta f_{\text{MW}}$, which is the expected response when driving at the fundamental.

Finally, we perform a spin echo experiment via second-harmonic driving. Figure 4(f) shows $P_\uparrow$ as a function of the total free evolution time τ, for a typical Hahn echo pulse sequence (illustrated in the inset) consisting of $\pi/2$, π, and

$\pi/2$ pulses applied along the same axis, separated by waiting times $\tau/2$ [41]. A fit to a single exponential yields $T_2^{\mathrm{echo}} = 20.6 \pm 6.5$ μs at $B_{\mathrm{ext}} = 560.783$ mT, compatible with the T_2^{echo} of 23.0 ± 1.2 μs we observed at the same magnetic field when driving via the fundamental harmonic (see Sec. I of [29]).

To summarize, we report coherent second-harmonic driving of an electron spin qubit defined in a Si/SiGe quantum dot, including universal single-spin rotations. The nonlinearity that permits second-harmonic driving is likely related to the anharmonic confining potential for the electron. This means that routine use of second harmonics for spin control would be possible provided there is sufficient control over the degree of anharmonicity of the confining potential. This could be very useful since driving a spin qubit at half its Larmor frequency would substantially simplify the microwave engineering required for high fidelity qubit control.

We acknowledge M. Rudner, A. Pályi, and T. Jullien for useful discussions, R. Schouten and M. J. Tiggelman for technical support. Research was supported by the Army Research Office (Grant No. W911NF-12-0607), the European Research Council and the Dutch Foundation for Fundamental Research on Matter. E. K. was supported by the Nakajima Foundation.

*Corresponding author.
L.M.K.Vandersypen@tudelft.nl

[1] D. Loss and D. P. DiVincenzo, Phys. Rev. A **57**, 120 (1998).
[2] R. Hanson, J. R. Petta, S. Tarucha, and L. M. K. Vandersypen, Rev. Mod. Phys. **79**, 1217 (2007).
[3] P. Franken, A. Hill, C. Peters, and G. Weinreich, Phys. Rev. Lett. **7**, 118 (1961).
[4] T. F. Heinz, C. K. Chen, D. Ricard, and Y. R. Shen, Phys. Rev. Lett. **48**, 478 (1982).
[5] Y. R. Shen, Nature (London) **337**, 519 (1989).
[6] W. Denk, J. H. Strickler, and W. W. Webb, Science **248**, 73 (1990).
[7] C. Xu, W. Zipfel, J. B. Shear, R. M. Williams, and W. W. Webb, Proc. Natl. Acad. Sci. U.S.A. **93**, 10763 (1996).
[8] K. Konig, J. Microsc. **200**, 83 (2000).
[9] S. Stufler, P. Machnikowski, P. Ester, M. Bichler, V. M. Axt, T. Kuhn, and A. Zrenner, Phys. Rev. B **73**, 125304 (2006).
[10] Y. Nakamura, Y. A. Pashkin, and J. S. Tsai, Phys. Rev. Lett. **87**, 246601 (2001).
[11] A. Wallraff, T. Duty, A. Lukashenko, and A. V. Ustinov, Phys. Rev. Lett. **90**, 037003 (2003).
[12] W. D. Oliver, Y. Yu, J. C. Lee, K. K. Berggren, L. S. Levitov, and T. P. Orlando, Science **310**, 1653 (2005).
[13] S. N. Shevchenko, A. N. Omelyanchouk, and E. Ilichev, Low Temp. Phys. **38**, 283 (2012).
[14] S. Poletto, J. M. Gambetta, S. T. Merkel, J. A. Smolin, J. M. Chow, A. D. Córcoles, G. A. Keefe, M. B. Rothwell, J. R. Rozen, D. W. Abraham *et al.*, Phys. Rev. Lett. **109**, 240505 (2012).
[15] A. De, C. E. Pryor, and M. E. Flatté, Phys. Rev. Lett. **102**, 017603 (2009).
[16] J. Pingenot, C. E. Pryor, and M. E. Flatté, Phys. Rev. B **84**, 195403 (2011).
[17] E. I. Rashba, Phys. Rev. B **84**, 241305 (2011).
[18] M. P. Nowak, B. Szafran, and F. M. Peeters, Phys. Rev. B **86**, 125428 (2012).
[19] E. N. Osika, A. Mrenca, and B. Szafran, Phys. Rev. B **90**, 125302 (2014).
[20] J. Danon and M. S. Rudner, Phys. Rev. Lett. **113**, 247002 (2014).
[21] J. Romhányi, G. Burkard, and A. Pályi, arXiv:1504.06081.
[22] G. Széchenyi and A. Pályi, Phys. Rev. B **89**, 115409 (2014).
[23] E. A. Laird, C. Barthel, E. I. Rashba, C. M. Marcus, M. P. Hanson, and A. C. Gossard, Semicond. Sci. Technol. **24**, 064004 (2009).
[24] F. Pei, E. A. Laird, G. A. Steele, and L. P. Kouwenhoven, Nat. Nanotechnol. **7**, 630 (2012).
[25] E. A. Laird, F. Pei, and L. P. Kouwenhoven, Nat. Nanotechnol. **8**, 565 (2013).
[26] J. Stehlik, M. D. Schroer, M. Z. Maialle, M. H. Degani, and J. R. Petta, Phys. Rev. Lett. **112**, 227601 (2014).
[27] S. Nadj-Perge, V. S. Pribiag, J. W. G. van den Berg, K. Zuo, S. R. Plissard, E. P. A. M. Bakkers, S. M. Frolov, and L. P. Kouwenhoven, Phys. Rev. Lett. **108**, 166801 (2012).
[28] F. Forster, M. Mühlbacher, D. Schuh, W. Wegscheider, and S. Ludwig, Phys. Rev. B **91**, 195417 (2015).
[29] See Supplemental Material at http://link.aps.org/supplemental/10.1103/PhysRevLett.115.106802 for extra and more in-depth information and data.
[30] E. Kawakami, P. Scarlino, D. R. Ward, F. R. Braakman, D. E. Savage, M. G. Lagally, M. Friesen, S. N. Coppersmith, M. A. Eriksson, and L. M. K. Vandersypen, Nat. Nanotechnol. **9**, 666 (2014).
[31] T. Obata, M. Pioro-Ladrière, Y. Tokura, Y.-S. Shin, T. Kubo, K. Yoshida, T. Taniyama, and S. Tarucha, Phys. Rev. B **81**, 085317 (2010).
[32] J. M. Elzerman, R. Hanson, L. H. Willems Van Beveren, B. Witkamp, L. M. K. Vandersypen, and L. P. Kouwenhoven, Nature (London) **430**, 431 (2004).
[33] J. K. Gamble, M. A. Eriksson, S. N. Coppersmith, and M. Friesen, Phys. Rev. B **88**, 035310 (2013).
[34] R. Boscaino, I. Ciccarello, C. Cusumano, and M. Strandberg, Phys. Rev. B **3**, 2675 (1971).
[35] I. Gromov and A. Schweiger, J. Magn. Reson. **146**, 110 (2000).
[36] Note that the ratio between the two Rabi frequencies is independent of the microwave amplitude in both cases, as we have $r_R(1\ \mathrm{ph}) = f_1^{(2)}/f_1^{(1)} = m_2 E_{\mathrm{ac}}/m_1 E_{\mathrm{ac}} = m_2/m_1$ and $r_R(2\ \mathrm{ph}) = f_1^{(4)}/f_1^{(3)} = q_4 E_{\mathrm{ac}}^2/q_3 E_{\mathrm{ac}}^2 = q_4/q_3$, respectively.
[37] R. Rahman, G. P. Lansbergen, S. H. Park, J. Verduijn, G. Klimeck, S. Rogge, and L. C. L. Hollenberg, Phys. Rev. B **80**, 165314 (2009).
[38] T. H. Oosterkamp, L. P. Kouwenhoven, A. E. A. Koolen, N. C. van der Vaart, and C. J. P. M. Harmans, Phys. Scr. **T69**, 98 (1997).
[39] E. Kawakami, P. Scarlino, L. R. Schreiber, J. R. Prance, D. E. Savage, M. G. Lagally, M. A. Eriksson, and L. M. K. Vandersypen, Appl. Phys. Lett. **103**, 132410 (2013).
[40] F. W. Strauch, S. K. Dutta, H. Paik, T. A. Palomaki, K. Mitra, B. K. Cooper, R. M. Lewis, J. R. Anderson, A. J. Dragt, C. J. Lobb *et al.*, IEEE Trans. Appl. Supercond. **17**, 105 (2007).
[41] E. Hahn, Phys. Rev. **80**, 580 (1950).